Hindawi
Journal of Food Quality
Volume 2018, Article ID 3873179, 8 pages
https://doi.org/10.1155/2018/3873179

Research Article

Effect of Storage Temperatures on the Moisture Migration and Microstructure of Beef

Xia Li,[1,2] Hang Wang,[1] Waris Mehmood,[1] Shuyi Qian,[3] Zhen Sun,[1] Chunhui Zhang,[1] and Christophe Blecker[2]

[1]*Institute of Food Science and Technology, Chinese Academy of Agricultural Sciences, Beijing 100193, China*
[2]*Unit of Food Science and Formulation, University of Liège, Gembloux Agro-Bio Tech, Passage des Déportés 2, Gembloux 5030, Belgium*
[3]*Institute of Biotechnology and Food Sciences, Tianjin University of Commerce, Tianjin 300134, China*

Correspondence should be addressed to Chunhui Zhang; dr_zch@163.com

Received 11 November 2017; Revised 30 April 2018; Accepted 14 May 2018; Published 21 June 2018

Academic Editor: Efstathios Giaouris

The effects of freezing temperature on the microstructure and moisture migration of beef were investigated, aiming to provide the potential theoretical basis for the beef storage. Drip loss, surface hydrophobicity, and secondary structure of myofibrillar proteins, ice crystal, and micro- and ultrastructure of meat were analyzed at 4°C, −1°C, −6°C, −9°C, −12°C, and −18°C, respectively. Results indicated that the drip loss and surface hydrophobicity of samples stored at −12°C were significantly lower than that stored at 4°C and −1°C ($p < 0.05$) and no significant difference with −18°C ($p > 0.05$). Result from Fourier transform infrared spectroscopy suggested that protein denaturation occurred after storage. There was an increase in α-helices and decline in random coil at lower temperature (−12°C and −18°C). It was indicated that the samples stored at −12°C and −18°C could effectively restrain the denaturation of protein and maintain the stability of secondary structure. The analysis of the ice crystal and micro- and ultrastructure of the muscle indicated that the structure of samples stored at −12°C and −18°C had more integrity and was complete than that stored at 4°C and −1°C. The spaces (water "reservoir" and "channel") where was the origination of drip were small. Furthermore, the results of low-field nuclear magnetic resonance and ^{1}H magnetic relaxation image showed that the freezing at −12°C could inhibit the migration of immobilized water to free water.

1. Introduction

Beef production and consumption are growing rapidly and emerging as an important source of protein in China to supply energy for humans due to rapid economic growth [1]. Meanwhile, frozen technology is vital to meat process and plays an important role during the circulation, sale, and storage [2]. Temperature and its fluctuation in the process of storage will absolutely influence the quality of frozen meat [2, 3]. Currently, the most common temperature used for meat preservation is from −18°C to −40°C [4]. However, it consumes high amount of energy, and temperature abuse occurs frequently. Furthermore, it takes long time in thawing which leads to inevitable deterioration in quality of meat during the process [5], such as weight decrease, color deterioration, flavour losses, texture changes, and high drip loss [6]. An appropriate freezing temperature is critical to maintain "fresh" meat quality to the largest extent.

Beef contains roughly 75% of the total muscle mass, which plays a vital role in meat and meat products [7]. About 85% of water content is located in the intramyofibrillar space and 15% of water content is present outside the myofibrillar network [8]. Water in the meat tissue could be characterized by three distinct populations (states): bound water, immobile water, and free water [9]. Therefore, the changes in the state of water will lead to significant effects on muscle structure and meat quality [10]. Low-field nuclear magnetic resonance (LF-NMR) has been effectively used to analyze the state, mobility, and distribution of water in meat. A new freezing temperature zone (−6°C to −12°C) of beef was

determined by LF-NMR, which falls between superchilling temperature (−1°C) and conventional freezing (−18°C). The effects of new temperature zone compared with conventional chilling (4°C), −1°C and −18°C, on the quality and storage time of beef were analyzed in our previous study. However, the effect of different frozen temperatures on the water mobility and distribution of beef is unclear. Since the structure of myofibrillar protein and muscle is crucial for holding water in meat [11], it is important to know how the freezing temperatures affect the physicochemical properties and structural changes of protein that contribute to water holding and migration of meat.

The objective of this study was to investigate the effects of different temperatures on the microstructure and moisture migration of beef after storage. Drip loss, surface hydrophobicity, secondary structure of myofibrillar proteins, ice crystal, and micro- and ultrastructure of meat were analyzed at 4°C, −1°C, −6°C, −9°C, −12°C, and −18°C, respectively.

2. Materials and Methods

2.1. Materials. Samples of bovine *longissimus dorsi* were obtained from a 2-year-old bull weighing 400 ± 5 kg (Simmental × Mongolian cattle, Zhuo Chen Animal Husbandry Co. Ltd, Beijing, China). Samples were cut into 50 mm* 50 mm* 50 mm pieces after removing the visible fats, ligaments, and tendons. Then, the samples were divided into two groups, one for the storage and other for low-field nuclear magnetic resonance (LF-NMR) analysis. The samples were assigned randomly to six groups and stored at 4°C (10 d), −1°C (24 d), −6°C (84 d), −9°C (126 d), −12°C (168 d), and −18°C (168 d), respectively. The storage time was decided according to the quality assessment of meat during storage. The drip loss, hydrophobicity, secondary structure of myofibrillar proteins, ice crystal, microstructures of myofibrillar proteins, and water mobility were determined after storage.

2.2. Drip Loss Analysis. Drip loss was measured according to the method described by Lan et al. with slight modifications [12]. Briefly, the initial sample weights were recorded before treatment. After storage, the samples were thawed at 4°C overnight and reweighed after wiping drips from their surface. The percentage of drip loss was calculated according to the following equation:

$$\text{drip loss}\,(\%) = \frac{\text{initial weight of raw material} - \text{weight after thawing}}{\text{initial weight of raw material} \times 100\%}. \quad (1)$$

2.3. Myofibrillar Proteins Preparation. Myofibrillar proteins were prepared from bovine *longissimus dorsi* according to the method of Park et al. and Li et al. [13, 14]. The purified myofibrillar protein isolate was stored in a tightly capped bottle and analyzed within 24 h. Protein concentration of the myofibril pellet was measured by the Biuret method using bovine serum albumin as the standard.

2.4. Hydrophobicity Analysis. Hydrophobicity of myofibrillar protein was determined using the hydrophobic chromophore bromophenol blue (BPB) according to the method of Chelh et al. [15]. The amount of bound BPB was expressed as the difference between total and free BPB and used as an index of hydrophobicity:

$$\text{bound BPB}\ (\mu\text{g}) = \frac{40\ \mu\text{g} \times (\text{OD control} - \text{OD sample})}{\text{OD control}}. \quad (2)$$

2.5. Secondary Structure of Myofibrillar Proteins Analysis. The secondary structure of myofibrillar proteins was analyzed by Fourier transform infrared (FTIR) spectrometer (Bruker Optics, Germany) according to the method of Li et al. [9] with modifications [10]. A Fourier transform infrared spectrometer equipped with MB-ATR (multibounce attenuated total reflectance) was used to obtain the spectra of myofibrillar protein. Samples of myofibrillar protein were scanned in 4000~400 cm^{-1} spectral. In order to improve the signal-to-noise ratio for each spectrum, a total of 64 scans at 4 cm^{-1} resolution were collected and each spectral map was scanned 100 times. Background spectra were subtracted using the Opus software. PEAKFIT 4.2 software was used to unscramble the amide I band, which ranges from 1600 to 1700 cm^{-1} spectrum.

2.6. Ice Crystal Observation. The ice crystal was observed according to the method of Kaale and Eikevik with modifications [16]. The samples were taken from the central part of each group sample, respectively, and cut along the muscle fiber direction using a surgical knife that was previously stored at each test temperature. Samples were about 10 mm in length and 5 mm* 5 mm in cross section and fixed using precooling stationary liquid (60% absolute ethanol, 30% chloroform, and 10% glacial acetic acid, v/v) for 20 h. The fixed samples were dehydrated using ethanol and *n*-butyl alcohol for 2 h at room temperature and then overnight in *n*-butyl alcohol. Paraffin-embedded samples were prepared under 60°C and cut into cubes and slices that are 5~10 μm thick by rotary microtome. After the samples were stained with hematoxylin-eosin, Olympus BX41 inverted biologic microscope (equipped with digital camera and image analysis software Image-Pro Plus 4.0 and 5.0) was used to shoot the typical image of the tissue.

2.7. Scanning Electron Microscope. The microstructures of the samples were observed by scanning electron microscope (SEM) according to the method of Li et al. [6]. The samples were cut into 3 mm* 3 mm* 5 mm and fixed with 3% glutaraldehyde overnight, rinsed 3 times in 0.1 M phosphate buffer (pH 7.2), and postfixed in 1% of osmium tetroxide at 4°C for 2 h before being dehydrated with graded ethanol. The dried samples were mounted on a bronze stub and

sputter-coated with gold (Eiko IB-5, Hitachi, Tokyo, Japan). The microstructures of samples were observed with SEM (Quanta 200 FEG, FEI, the Netherlands) at a magnification of 500x.

2.8. Transmission Electron Microscopy. The microstructures of the samples were observed by transmission electron microscope (TEM) according to the method of Li et al. [6]. The samples were cut into 4 mm* 4 mm* 2 mm and fixed with 2.5% glutaraldehyde, rinsed in the 0.1 M phosphate buffer (pH 7.4), and postfixed in 1% of osmium tetroxide at 4°C for 2 h before being dehydrated with graded ethanol and acetone. The samples were later embedded in Spurr's resin, and sections were stained with both lead citrate and uranyl acetate. The ultrastructures of samples were observed with TEM (H-7500, Hitachi, Japan) at a magnification of 25,000x.

2.9. Water Mobility Analysis. The NMR probe for spin-spin relaxation time (T_2) was used. The T_2 values of the water protons in the samples were measured on a 0.5-Tesla magnet (PQ-001, Niumag Electric Corporation, Shanghai, China) using the Carr–Purcell–Meiboom–Gill (CPMG) sequences by biexponential fitting of the data to a linear combination of three exponentials in terms of relaxing time constant T_{21}, T_{22}, and T_{23}. The measurements were taken at 32°C. The τ-value (time between 90° pulse and 180° pulse) was 200 μs. Data from 8,000 echoes were acquired as four scan repetitions for each sample. The repetition time between the two succeeding scans was 1,000 ms. The multiexponential decay curve was obtained from NMR relaxation measurement using the mathematical model as follows:

$$A(t) = \sum_i A_{0i} \exp\left(\frac{-t}{T_{2i}}\right), \quad (3)$$

where $A(t)$ is the amplitude size when attenuation to t; A_{0i} is the amplitude size when the first component balance; t is the decay time; and T_{2i} is the relaxation time of the I relaxation component. Distributed multiexponential fitting of CPMG decay curves were performed using MultiExpInv Analysis software (Niumag Electric Corporation, Shanghai, China). P_{21}, P_{22}, and P_{23} were used to represent the percentages of T_{21}, T_{22}, and T_{23}, respectively. P_{21}, P_{22}, and P_{23} (the areas under each peak) were determined by cumulative integration.

2.10. Proton Density Images Analysis. The proton density images of samples were stored through different methods and scanned using a MINI MR-60 instrument (Niumag Electric Corporation, Shanghai, China). The magnetic relaxation image (MRI) measurements were acquired as proton density images using MSE imaging sequence with the following parameters: time to repetition (TR) = 800 ms, time to echo (TE) = 18.2 ms, center frequency (SF) = 23.319 MHz, field of view (FOV) read = 50 mm, and FOV phase 50 mm. The samples were divided into four layers for analysis; the width of each layer was 1.8 mm, and slice gap was 0.5 mm.

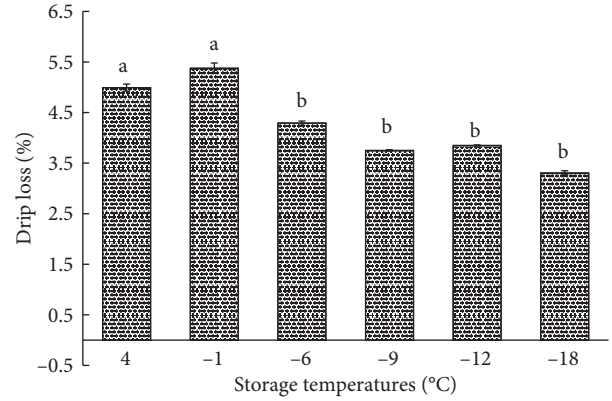

Figure 1: Changes of drip loss at different storage temperatures. Values are expressed as mean ± standard deviation. Same letters above the bars indicate no significant difference ($p > 0.05$).

Each image was acquired as a sum of eight scans. Images were converted to a BMP image format. Arbitrary color-scale surface plots were used to represent the distribution of water within the samples. The distribution of grey scale intensities in the MR images was analyzed using the Image Evaluation computer software (Shanghai Niumag Corporation).

2.11. Statistical Analysis. All experiments were carried out at least in triplicate, and the values given below were the means of these triplicates except FTIR. Statistical analyses were performed using SPSS version 19.0 (SPSS Inc., Chicago, IL, USA). Significant differences were analyzed using one-way ANOVA and Duncan's multiple-range test at a significance level of 0.05.

3. Results and Discussion

3.1. Drip Loss Analysis. The results of the drip loss are presented in Figure 1. The mean values of drip loss of the samples at different temperatures were around 3.31%–4.92%. Higher amounts of drip loss were observed in the group at 4°C and −1°C ($p < 0.05$). The drip loss of samples treated at the test temperature (−6, −9, and −12°C) was significantly lower ($p < 0.05$) than that of samples treated at 4°C and −1°C. In addition, there were no significant differences ($p > 0.05$) between the drip loss of samples which were frozen at −12°C and −18°C. It was indicated that samples treated at −12°C could maintain the WHC of samples effectively. In this study, the drip loss of samples corresponded with the reduction in hydrophobicity (Figure 2).

3.2. Protein Surface Hydrophobicity Analysis. Surface hydrophobicity can be a suitable parameter to estimate protein denaturation, and higher protein surface hydrophobicity represents more protein denaturation [17]. As shown in Figure 2, surface hydrophobicity of myofibrillar protein changed significantly at different temperatures (4, −1, −6, −9, −12, and −18°C). The surface hydrophobicity of samples stored at −12°C and −18°C was significantly lower ($p < 0.05$)

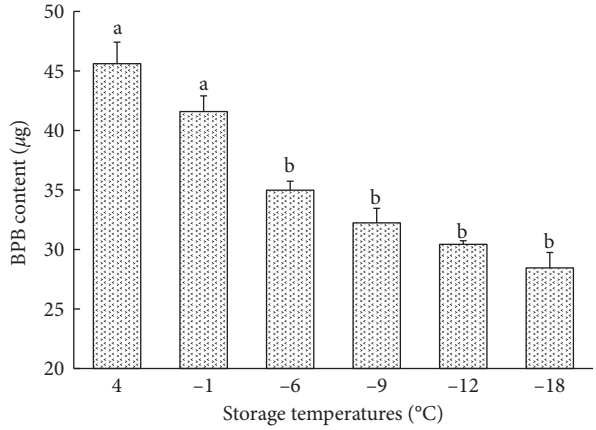

Figure 2: Surface hydrophobicity of myofibrillar protein at different storage temperatures. Values are expressed as mean ± standard deviation. Same letters above the bars indicate no significant difference ($p > 0.05$).

than that of samples at 4°C and −1°C. The BPB content of −12°C at day 168 was $30.43 \pm 0.16\,\mu g$, which had no significant differences ($p < 0.05$) with the −18°C method, of which the BPB content is $28.45 \pm 0.37\,\mu g$ at day 168. It was suggested that the storage at −12°C has an effective inhibitory action to protein surface hydrophobicity. The difference of surface hydrophobicity was due to conformation changes that are hydrogen bonds and disulfide bonds [17]. Bound water that connected with protein and part of immobilized water easily transformed into free water, which causes the increase of drip loss. The results of surface hydrophobicity were consistent with the drip loss and the LF-NMR (Figure 1; Table 1 and Figure 7).

3.3. Secondary Structure of Myofibrillar Proteins Analysis. FTIR was used to scan all the wave bands (400~4000 cm^{-1}) of samples. Multiple characteristic absorption bands will be formed in the infrared region, among which the amide I is located in the 1600~1700 cm^{-1} wave band [18], which is led by the stretching vibration of C = O. The wave band ranging from 1615~1637 cm^{-1} and 1682~1700 cm^{-1} is called β-sheet, 1646~1664 cm^{-1} is called α-helix, 1637~1645 cm^{-1} is called random coil, and 1664~1681 cm^{-1} is called β-turn [19]. As shown in Figure 3, the content of α-helix presented an increased trend from 4°C to −18°C ($p < 0.05$), while the content of β-sheet and β-turn was quite similar. And content of random coil at −12°C and −18°C was slightly higher than 4°C and −1°C. The stabilized α-helix structures were maintained by hydrogen bonds between –CO and NH– of a polypeptide chain [20]. The reduction of α-helix at 4°C and −1°C illustrated that the stability of the secondary structure of myofibrillar protein like hydrogen bonds would be damaged. And the hydrophobic group that was expected to be inside the protein is exposed to the surface, which increased the protein surface hydrophobicity. These results were expected to explain the reduced drip loss and surface hydrophobicity at −12°C and −18°C.

Table 1: LF-NMR-T_2 analysis of beef three water populations over different storage temperatures.

Storage temperatures	P_{21} (%)	P_{22} (%)	P_{23} (%)
4°C	1.47 ± 0.21b	96.55 ± 0.34b	2.46 ± 0.05a
−1°C	1.70 ± 0.11a	96.32 ± 0.27b	1.98 ± 0.31b
−6°C	1.42 ± 0.30b	96.08 ± 0.93c	1.50 ± 0.63c
−9°C	1.36 ± 0.15bc	97.18 ± 1.14a	1.46 ± 0.17c
−12°C	1.58 ± 0.05ab	96.54 ± 0.35b	1.28 ± 0.13d
−18°C	1.37 ± 0.02bc	97.26 ± 0.13a	1.27 ± 0.09d

Note. The data in the table are the average value ± standard deviation; a, b, c, and so on in the same column express that there are significant differences between different treatment groups ($p < 0.05$).

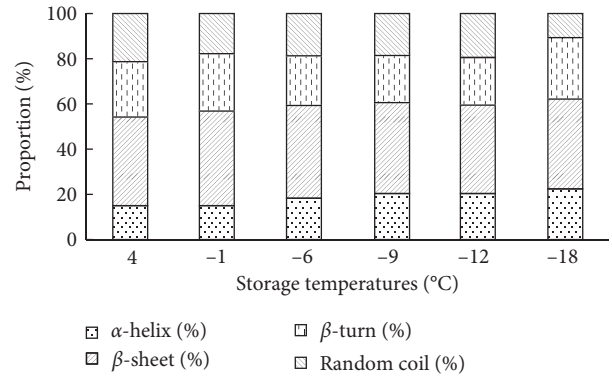

Figure 3: Secondary structure relative contents of beef myofibrillar protein at different temperatures.

3.4. Ice Crystal Observation. Both the amount and volume of ice crystals increased during frozen storage. The muscle cell would be squeezed seriously by ice crystal growth and caused irreversible influences [21]. The muscle cell could hardly recover to their original status even after thawing and formed a "reservoir" and "channel". Figure 4 shows the ice crystal distribution of samples in different groups. Muscle bundles shrink, and obvious gaps and holes were observed in tissues after frozen storage. The gaps found while storage at −6°C were obviously larger than samples at −9, −12, and −18°C, respectively. It was suggested that the ice crystal growth at −6°C samples was faster than the other 3 groups, causing even greater damage to the muscle tissues. Meanwhile, the volume of ice crystals at −12°C and −18°C had no significant difference. Muscle integrity can be maintained at −12°C and −18°C, which was consistent with the results of microstructure. Therefore, sample stored at −12°C and −18°C showed higher water-holding capacity.

3.5. Microstructure Observation. Current study analyzed the changes in the microstructures of muscle fibers at different storage temperatures by SEM and TEM. Muscle fibers of the 4°C and −1°C shrink critically after storage (Figure 5). The gap between fiber bundles was widened and exomysium was seriously fractured and separated. Diameter of muscle fibers in the two groups was enlarged and the structural integrity of the muscle fiber bundle was damaged. The loose structure and expanded muscle fiber structures cause the declining in

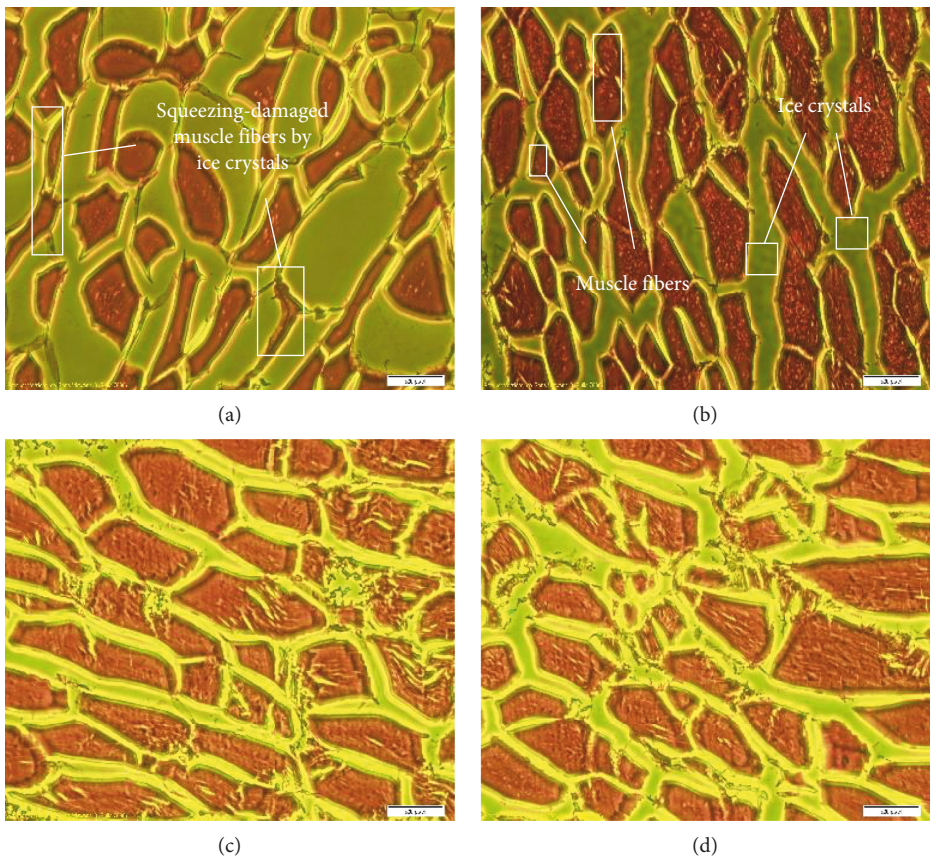

Figure 4: Ice crystal observation of beef muscle stored at (a) −6°C, (b) −9°C, (c) −12°C, and (d) −18°C.

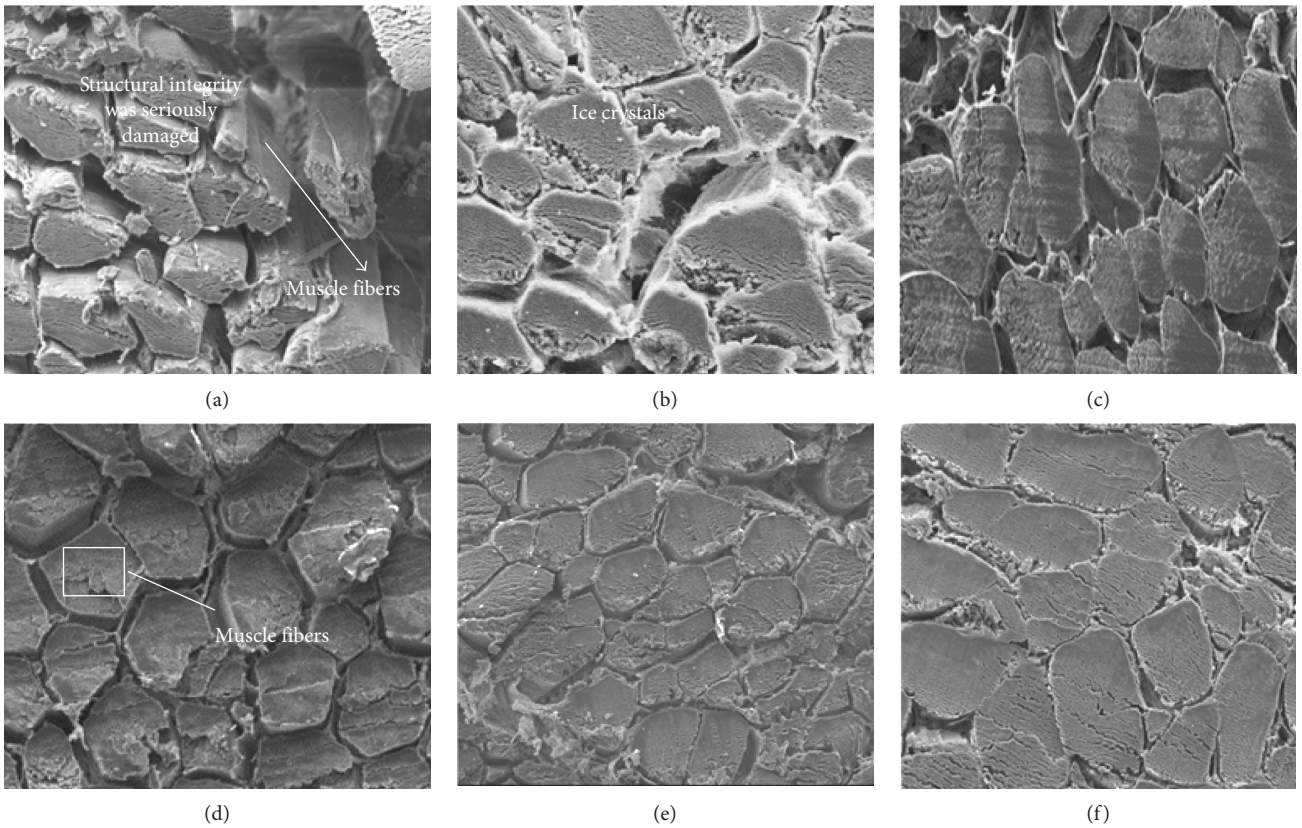

Figure 5: The effects of different storage temperatures on microstructure of beef muscle at (a) 4°C, (b) −1°C, (c) −6°C, (d) −9°C, (e) −12°C, and (f) −18°C by scanning electron microscopy (magnification ×500).

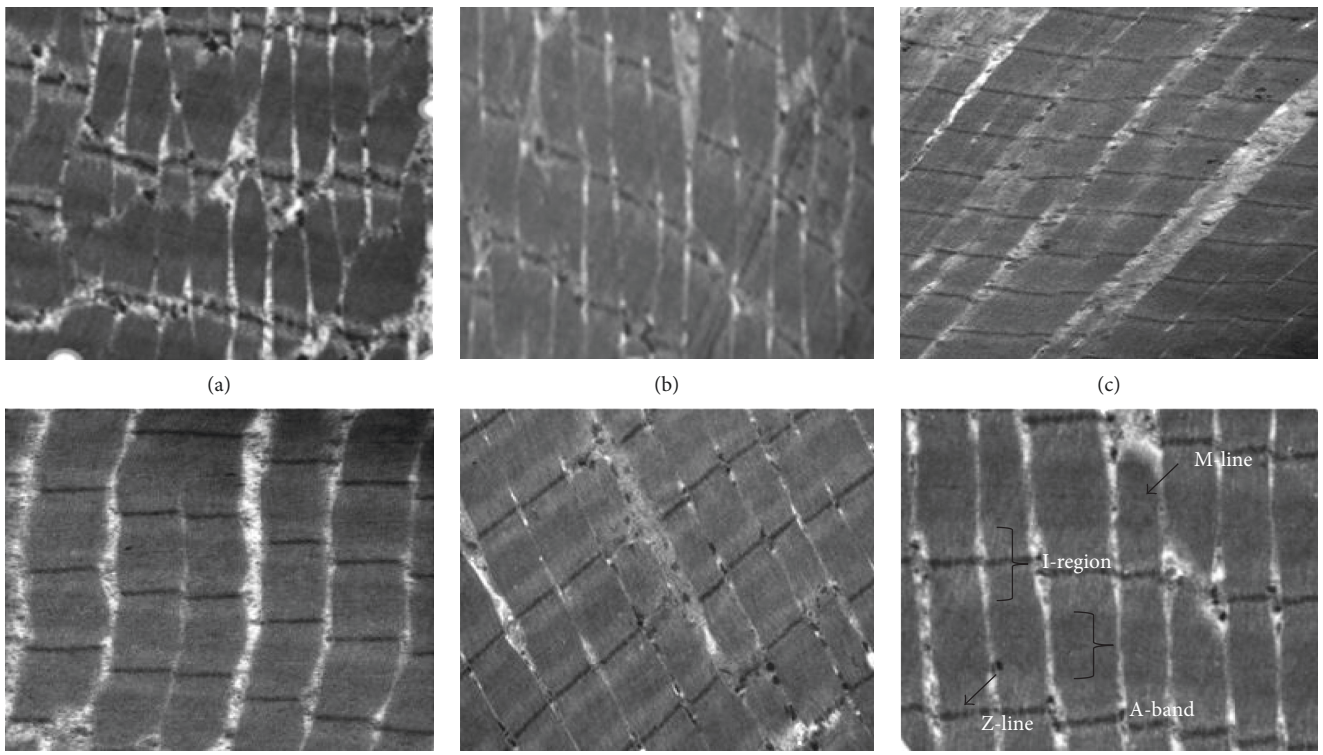

(a) (b) (c)

(d) (e) (f)

Figure 6: The effect of different storage temperatures on ultrastructure of beef muscle at (a) 4°C, (b) −1°C, (c) −6°C, (d) −9°C, (e) −12°C, and (f) −18°C by transmission electron microscopy (magnification ×25,000).

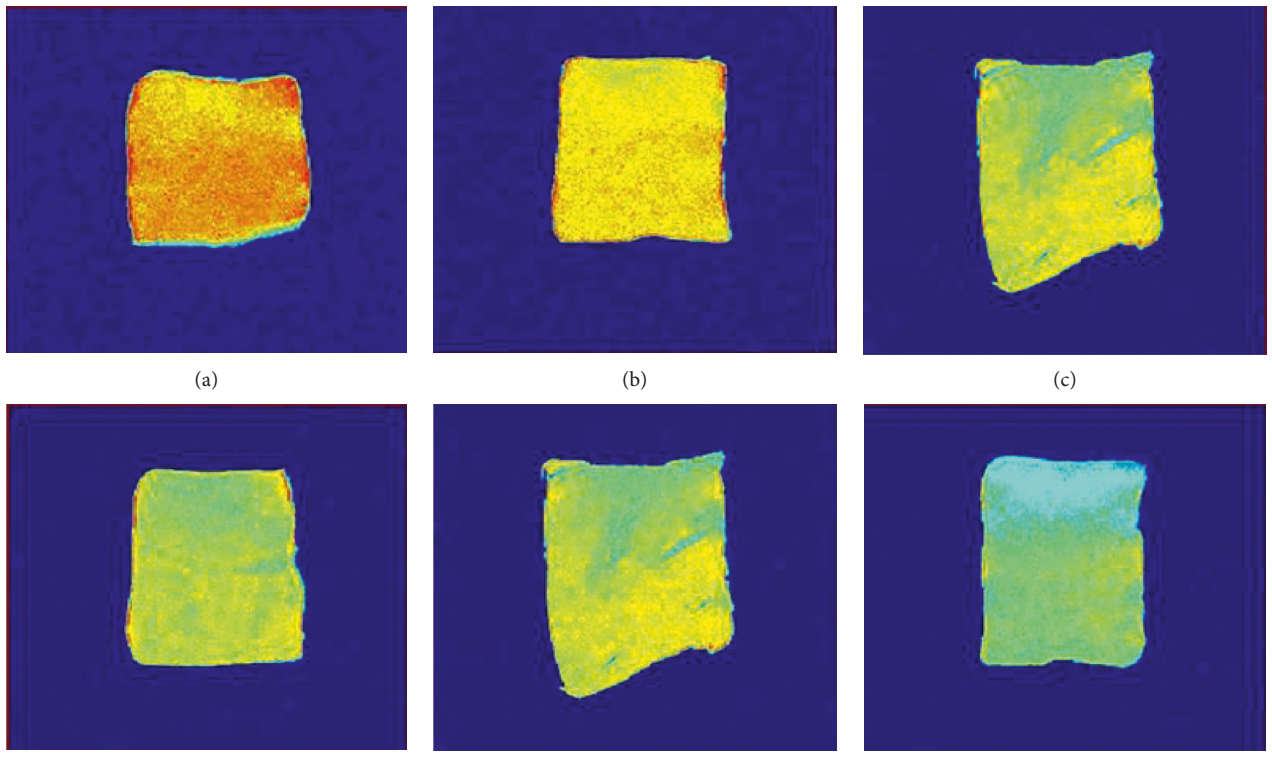

(a) (b) (c)

(d) (e) (f)

Figure 7: Effect of different storage temperatures on the H-proton density image of beef muscle at (a) 4°C, (b) −1°C, (c) −6°C, (d) −9°C, (e) −12°C, and (f) −18°C.

water-holding capacity, which ultimately leads to drip loss and deterioration of meat structure. The gaps between fiber bundles at −6°C and −9°C groups were widened due to the shrinkage of muscle fibers, but the exomysium was not fractured. Compared to the other groups, the muscle fiber structures of samples stored at −12°C and −18°C were more compact and well preserved, ensuring better water-holding capacity.

The TEM diagram of microstructures by the end of each storage condition is shown in Figure 6. Muscle fibers were composed of multiple sarcomeres, and each sarcomere included 2 Z-lines (the region between two neighboring Z-lines was called one sarcomere). Sarcomere was the basic contractile unit of muscle, and the length of sarcomere was positively correlated with the water-holding capacity of muscles [6]. The muscle fiber structures of samples stored at 4°C and −1°C were uneven with sarcomere dislocation, and Z-line disintegration. A-bands, I-bands, and Z-lines in Figure 6 are obvious. The results showed that the sarcomere shortening, light Z-lines distorting, and the bandings were less regular than that of samples stored at −12°C and −18°C. Some spaces would be formed due to the results. The drip was discharged from the spaces and formed drip loss.

3.6. Water Mobility Analysis. The change of muscle fiber structure leads to the migration of the muscle water distribution during storage. Based on LF-NMR results, the water in samples was characterized by three forms: bound water (0.1~10 ms), immobilized water (10~100 ms), and free water (100~1000 ms) [22, 23]. The relative percentages of the three waters were represented as P_{21}, P_{22}, and P_{23}, and the results are shown in Table 1.

P_{21} was rather low, and no significant differences ($p < 0.05$) were found among these groups, which means that the storage has little influence on the bound water in samples. This result was consistent with the findings reported by [24]. The result of P_{22} showed that samples in 4°C and −1°C groups had significantly lower content of immobilized water ($p < 0.05$) compared to the samples stored at −6, −9, −12 and −18°C groups. Contrary to the content of immobilized water, the free water content (P_{23}) of 4°C and −1°C groups was significantly higher ($p < 0.05$) than the other groups. The results suggested that the frozen state of −6, −9, and −12°C was nearly the same and particularly, no significant difference ($p > 0.05$) was found between free water content of −12°C and −18°C.

3.7. Proton Density Images of Muscle Analysis. MRI can readily show the distribution of H-proton inside the tested materials without damaging the proton [25, 26]. The deeper red color represents higher H-proton density, and the deeper blue color stands for lower H-proton density [27]. As shown in Figure 7, image colors of the samples showed obvious changes after thawing. The 4°C group had the most region of red color, which means it had the highest H-proton density (means it had the highest free water content); the −1°C group ranks the second, and then followed by −6, −9, −12, and −18°C groups. The images of samples stored at −12°C and −18°C showed a rather blue color, which means that, compared to other groups, the free water content was lower, and water migration was slower in these two groups. The hydrogen proton density images were in agreement with LF-NMR results.

4. Conclusions

Freezing at −12°C and −18°C could effectively reduce the denaturation of beef protein. It showed the increase in α-helices and decline in random coil for samples stored at −12°C and −18°C, suggesting a stable secondary structure and increased water-holding capacity. Moreover, freezing at lower temperatures could inhibit the migration of immobilized water to free water.

Conflicts of Interest

The authors declare that there are no conflicts of interest regarding the publication of this article.

Acknowledgments

The authors would like to thank National Natural Science Foundation of China for funding this research (Grant nos. 31571787 and 31671789).

References

[1] D. L. Ortega, S. J. Hong, H. H. Wang, and L. Wu, "Emerging markets for imported beef in China: results from a consumer choice experiment in Beijing," *Meat Science*, vol. 121, no. 11, pp. 317–323, 2016.

[2] Q. Liu, R. Wang, B. H. Kong, and Y. G. Zhang, "Effect of superchilling storage on quality characterizes of beef as compared with chilled and frozen preservation," *Advanced Materials Research*, vol. 554–556, pp. 1195–1201, 2012.

[3] M. M. Farouk, R. M. Kemp, S. Cartwright, and M. North, "The initial freezing point temperature of beef rises with the rise in pH: a short communication," *Meat Science*, vol. 94, no. 1, pp. 121–124, 2013.

[4] E. Muela, C. Saňudo, M. M. Campo, I. Medel, and J. A. Beltrán, "Effect of freezing method and frozen storage duration on instrumental quality of lamb throughout display," *Meat Science*, vol. 84, no. 4, pp. 662–629, 2010.

[5] J. S. Eastridge and B. C. Bowker, "Effect of rapid thawing on the meat quality attributes of USDA select beef strip loin steaks," *Journal of Food Science*, vol. 76, no. 2, pp. S156–S162, 2015.

[6] Y. Li, W. Jia, C. H. Zhang et al., "Fluctuated low temperature combined with high-humidity thawing to reduce physicochemical quality deterioration of beef," *Food and Bioprocess Technology*, vol. 7, no. 12, pp. 3370–3380, 2014.

[7] J. Estrada-Solís, K. A. Figueroa-Rodríguez, B. Figueroa-Sandoval, F. Hernández-Rosas, and A. S. Hernández-Cazares, "Microstructure and physical changes in the Mexican cooked lamb meat barbacoa made with chilled and frozen meat," *Meat Science*, vol. 118, no. 4, pp. 122–128, 2016.

[8] X. Li, C. Xie, S. Zhang, S. Zhen, and W. Jia, "Role of mid- and far-infrared for improving dehydration efficiency in beef jerky drying," *Drying Technology*, vol. 36, no. 3, pp. 283–293, 2018.

[9] X. Li, X. Wei, H. Hang, C. H. Zhang, and W. Mehmood, "Relationship between protein denaturation and water

holding capacity of pork during postmortem ageing," *Food Biophysics*, vol. 13, no. 1, pp. 18–24, 2018.

[10] F. T. Ndoye and G. Alvarez, "Characterization of ice recrystallization in ice cream during storage using the focused beam reflectance measurement," *Journal of Food Engineering*, vol. 148, no. 3, pp. 24–34, 2015.

[11] J. M. Hughes, S. K. Oiseth, P. P. Purslow, and R. D. Warner, "A structural approach to understanding the interactions between colour, water-holding capacity and tenderness," *Meat Science*, vol. 98, no. 3, pp. 520–532, 2014.

[12] Y. Lan, Y. Shang, Y. Song, and Q. Dong, "Changes in the quality of superchilled rabbit meat stored at different temperatures," *Meat Science*, vol. 117, no. 7, pp. 173–181, 2016.

[13] D. Park, Y. L. Xiong, and A. L. Alderton, "Concentration effects of hydroxyl radical oxidizing systems on biochemical properties of porcine muscle myofibrillar protein," *Food Chemistry*, vol. 101, no. 3, pp. 1239–1246, 2007.

[14] Y. Li, X. Li, J.-Z. Wang et al., "Effects of oxidation on water distribution and physicochemical properties of porcine myofibrillar protein gel," *Food Biophysics*, vol. 9, no. 2, pp. 169–178, 2014.

[15] I. Chelh, P. Gatellier, and V. Santé-Lhoutellier, "Technical note: a simplified procedure for myofibril hydrophobicity determination," *Meat Science*, vol. 74, no. 4, pp. 681–683, 2006.

[16] L. D. Kaale and T. M. Eikevik, "A study of the ice crystal sizes of red muscle of pre-rigor Atlantic salmon (*Salmo salar*) fillets during superchilled storage," *Journal of Food Engineering*, vol. 119, no. 3, pp. 544–551, 2013.

[17] V. Santé-Lhoutellier, T. Astruc, P. Marinova, E. Greve, and P. Gatellier, "Effect of meat cooking on physicochemical state and in vitro digestibility of myofibrillar proteins," *Journal of Agricultural and Food Chemistry*, vol. 56, no. 4, pp. 1488–1494, 2008.

[18] J. H. Cheng and D. W. Sun, "Recent applications of spectroscopic and hyperspectral imaging techniques with chemometric analysis for rapid inspection of microbial spoilage in muscle foods," *Comprehensive Reviews in Food Science and Food Safety*, vol. 14, no. 4, pp. 478–490, 2015.

[19] V. C. Schmidt, C. Giacomelli, and V. Soldi, "Thermal stability of films formed by soy protein isolate-sodium dodecyl sulfate," *Polymer Degradation and Stability*, vol. 87, no. 1, pp. 25–31, 2005.

[20] T. Sano, T. Ohno, H. Otsukafuchino, J. J. Matsumoto, and T. Tsuchiya, "Carp natural actomyosin: thermal denaturation mechanism," *Journal of Food Science*, vol. 59, no. 5, pp. 1002–1008, 2010.

[21] M. N. Martino and N. E. Zaritzky, "Ice crystal size modifications during frozen beef storage," *Journal of Food Science*, vol. 53, no. 6, pp. 1631–1637, 2010.

[22] I. Sánchez-Alnso, P. Moreno, and M. Careche, "Low field nuclear magnetic resonance (LF-NMR) relaxometry in hake (*Merluccius merluccius*, L.) muscle after different freezing and storage conditions," *Food Chemistry*, vol. 153, no. 12, pp. 250–257, 2014.

[23] M. Zhang, F. Li, X. Diao, B. Kong, and X. Xia, "Moisture migration, microstructure damage and protein structure changes in porcine longissimus muscle as influenced by multiple freeze-thaw cycles," *Meat Science*, vol. 133, no. 11, pp. 10–18, 2017.

[24] J. H. Shao, Y. M. Deng, L. Song, A. Batur, N. Jia, and D. Y. Liu, "Investigation the effects of protein hydration states on the mobility water and fat in meat batters by LF-NMR technique," *LWT-Food Science and Technology*, vol. 66, no. 3, pp. 1–6, 2016.

[25] H. M. Lai and S. C. Hwang, "Water status of cooked white salted noodles evaluated by MRI," *Food Research International*, vol. 37, no. 10, pp. 957–966, 2004.

[26] H. Martens, A. K. Thybo, H. J. Andersen et al., "Sensory analysis for magnetic resonance-image analysis: using human perception and cognition to segment and assess the interior of potatoes," *LWT-Food Science and Technology*, vol. 35, no. 1, pp. 70–79, 2002.

[27] H. Shyh-Shin, Y.-C. Cheng, C. Chen, H.-S. Lur, and T.-T. Lin, "Magnetic resonance imaging and analyses of tempering processes in rice kernels," *Journal of Cereal Science*, vol. 50, no. 1, pp. 36–42, 2009.